



1 Temporary pause in the growth of atmospheric ethane and 2 propane in 2015-2018

3 **Hélène Angot^{1,2}, Connor Davel¹, Christine Wiedinmyer³, Gabrielle Pétron^{3,4}, Jashan**
4 **Chopra¹, Jacques Hueber^{1,5}, Brendan Blanchard¹, Ilann Bourgeois^{3,6}, Isaac Vimont³,**
5 **Stephen A. Montzka⁴, Ben R. Miller^{3,4}, James W. Elkins⁴, Detlev Helmig^{1,5}.**

6 ¹Institute of Arctic and Alpine Research, University of Colorado Boulder, Boulder, CO, USA.

7 ²School of Architecture, Civil and Environmental Engineering, École Polytechnique Fédérale de Lausanne, Sion,
8 Switzerland.

9 ³Cooperative Institute for Research in Environmental Sciences, University of Colorado Boulder, Boulder, CO, USA.

10 ⁴NOAA, Global Monitoring Laboratory (GML), Earth System Research Laboratories, Boulder, CO, USA.

11 ⁵Boulder A.I.R. LLC, Boulder, CO, USA.

12 ⁶NOAA, Chemical Sciences Laboratory (CSL), Earth System Research Laboratories, Boulder, CO, USA.

13 *Correspondence to:* Hélène Angot (helene.angot@epfl.ch)

14 **Abstract.**

15 Atmospheric non-methane hydrocarbons (NMHCs) play an important role in the formation of
16 secondary organic aerosols and ozone. After a multidecade global decline in atmospheric mole
17 fractions of ethane and propane – the most abundant atmospheric NMHCs – previous work has
18 shown a reversal of this trend with increasing atmospheric abundances from 2009 to 2015 in the
19 Northern Hemisphere. These concentration increases were attributed to the unprecedented growth
20 in oil and natural gas (O&NG) production in North America. Here, we supplement this trend
21 analysis building on the long-term (2008-2010; 2012-2020) high-resolution (~ 3-hour) record of
22 ambient air C₂-C₇ NMHCs from in-situ measurements at the Greenland Environmental
23 Observatory at Summit station (GEOSummit, 72.58°N, 38.48°W, 3210 m above sea level). We
24 confirm previous findings that the ethane mole fraction significantly increased by +69.0 [+47.4,
25 +73.2; 95 % confidence interval] ppt per year from January 2010 to December 2014. Subsequent
26 measurements, however, reveal a significant decrease by -58.4 [-64.1, -48.9] ppt per year from
27 January 2015 to December 2018. A similar reversal is found for propane. The upturn observed
28 after 2019 suggests, however, that the pause in the growth of atmospheric ethane and propane
29 might only have been temporary. The analysis of 2012-2019 air mass back-trajectories shows that
30 this pause in mole fraction increases can neither be attributed to changes in atmospheric transport



31 nor to changes in regional emissions. Discrete samples collected at other northern-hemisphere
32 baseline sites under the umbrella of the NOAA cooperative global air sampling network show a
33 similar decrease in 2015-2018 and suggest a hemispheric pattern. Here, we further discuss the
34 potential contribution of biomass burning and O&NG emissions, the main sources of ethane and
35 propane, and we conclude that O&NG activities likely played a role in these recent changes. This
36 study, however, highlights the crucial need for better constrained emission inventories.

37

38 **1. Introduction**

39 Non-methane hydrocarbons (NMHCs) are emitted to the atmosphere by a variety of biogenic and
40 anthropogenic sources. Their atmospheric oxidation contributes to the production of surface ozone
41 and aerosols, with impacts on air quality and climate forcing (Houweling et al., 1998). The
42 abundance of the most abundant atmospheric NMHCs (ethane, propane, i-butane, n-butane, i-
43 pentane, n-pentane) increased steadily after 1950 until reduced emissions from oil and natural gas
44 (O&NG) production and emission regulations from diverse sources (e.g., automobiles and
45 industrial processes) began to be implemented in the 1970s (Helmig et al., 2014). Emission
46 reductions led to a gradual decline (3-12 % per year) of NMHCs at urban and semi-rural sites in
47 the last five decades (e.g., von Schneidemesser et al., 2010; Warneke et al., 2012). Accounting for
48 an approximate atmospheric lifetime (at $\text{OH} = 6.5 \times 10^5 \text{ molecules/cm}^3$) ranging from 4.5 days
49 for pentanes to 2 months for ethane, these emission reductions are also reflected in observations
50 of background air composition, as seen in Northern Hemisphere firm air records (Aydin et al., 2011;
51 Worton et al., 2012; Helmig et al., 2014): light alkanes increased steadily post 1950, peaking ~50
52 % above 1950 levels around 1970-1985, and then steadily declined until 2010 to levels that were
53 close to 1950 levels. After some 40 years of steadily declining atmospheric ethane and propane
54 mixing ratios, Helmig et al. (2016) reported a reversal in this behavior: the analysis of weekly
55 discrete air samples has shown that between mid-2009 and mid-2014, ethane abundance at surface
56 sites in the Northern Hemisphere increased at a rate of 2.9-4.7 % per year. These observations and
57 conclusions were further substantiated by solar Fourier transform infrared (FTIR) ethane column
58 retrievals showing similar increases in the mid to upper tropospheric ethane column (Franco et al.,
59 2015, 2016; Hausmann et al., 2016). The largest increase rates for ethane and propane mixing
60 ratios were found at sites located in the Eastern United States (U.S.) and in the Northern Atlantic



61 Region, indicating larger emissions from the central to eastern parts of the U.S., with the likely
62 sources being increased emissions from shale O&NG extraction operations.

63 Interestingly, there is a strong latitudinal gradient of absolute NMHC dry air mole fractions – with
64 highest abundances in the Arctic where atmospheric removal rates are low during the polar winter
65 (Helmig et al., 2016, 2009; Rudolph, 1995). Despite the sensitivity of the Arctic to pollution
66 transport from lower latitudes, climate change, and already recognized and further anticipated
67 feedbacks on the global climate, long-term in-situ atmospheric composition observations within
68 the Arctic are sparse. A large part of our current knowledge of polar atmospheric chemistry stems
69 from research aircraft missions and campaign-type observations (e.g., Hartery et al., 2018; Jacob
70 et al., 2010; Law et al., 2014). However, long-term continuous measurements or regularly repeated
71 observations with consistent methodology and instrumentation are indispensable for establishing
72 a baseline record of environmental conditions at clean remote sites and for observing their changes
73 over time. Such data also serve as a legacy for future research that will rely on comparison with
74 archived observations of environmental conditions.

75 In that context, the National Oceanic and Atmospheric Administration (NOAA) Global
76 Monitoring Laboratory (GML) initiated a cooperative air-sampling network at Niwot Ridge,
77 Colorado, in 1967 (hereafter referred to as the NOAA/GML Carbon Cycle Greenhouse Gases
78 (CCGG) network (<https://www.esrl.noaa.gov/gmd/ccgg/>)). This network is nowadays an
79 international effort and discrete air samples are collected approximately weekly from a globally
80 distributed network of sites, including four Arctic sites: Utqiagvik (formerly known as Barrow,
81 Alaska, USA), Alert (Nunavut, Canada), Summit (Greenland), and Ny-Ålesund (Svalbard,
82 Norway). These samples are analyzed for CO₂, CH₄, CO, H₂, N₂O, and SF₆ at GML (e.g., Geller
83 et al., 1997; Komhyr et al., 1985; Steele, 1991), at the University of Colorado Institute for Arctic
84 and Alpine Research (INSTAAR) for stable isotopes of CO₂ and CH₄ (Miller et al., 2002; Trolier
85 et al., 1996), and, since 2004, for a variety of volatile organic compounds (VOCs) including C₂-
86 C₇ NMHCs (Pollmann et al., 2008; Schultz et al., 2015). Since 2014, measurements of ethane and
87 propane were added to discrete air samples collected under the umbrella of the NOAA/GML
88 Halocarbons and other Atmospheric Trace Species (HATS) network since 2004
89 (<https://www.esrl.noaa.gov/gmd/hats/flask/flasks.html>).

90 The discrete, typically weekly, air sampling by cooperative global networks have been at the
91 forefront of studies to identify and quantify long-term trends in the background air abundances of



92 important trace gases (e.g., Masarie and Tans, 1995; Montzka et al., 2018; Nisbet et al., 2014,
93 2019). In parallel, higher temporal-resolution in-situ measurements allow the investigation of
94 source regions and of shorter-term trends at specific sites. Here, we report in-situ 2 to 4-hourly
95 ambient air C₂-C₇ NMHCs dry air mole fractions from measurements at the Greenland
96 Environmental Observatory at Summit station (GEOSummit) by gas chromatography (GC) and
97 flame ionization detection (FID). Despite the advent of new methods based on optical
98 measurement (e.g., FTIR spectroscopy) and mass spectrometry (e.g., Photon-Transfer Mass
99 Spectrometry), GC-FID remains the dominant method in routine VOC observations due to its
100 stable long-term response characteristics and relatively low maintenance cost (Schultz et al., 2015).
101 NMHCs were first monitored with high temporal frequency at GEOSummit from 2008 to 2010
102 with support from the NASA Research Opportunities in Space and Earth Sciences (ROSES)
103 program (Kramer et al., 2015). NMHC monitoring resumed in 2012 as part of the National Science
104 Foundation (NSF) Arctic Observing Network program and has been continuous and uninterrupted
105 until March 2020, providing one of the few high-temporal resolution long-term records of NMHCs
106 in the Arctic. In this paper, we investigate and discuss seasonal variations, rates of change, and
107 potential sources of NMHCs in the high Arctic. We also analyze multiyear trace gas data from
108 other background sites under the umbrella of the NOAA/GML CCGG and HATS sampling
109 networks to support our findings.

110

111 **2. Materials and Methods**

112 GEOSummit (72.58°N, 38.48°W, 3210 m above sea level) is a research facility located on the
113 Greenland ice sheet funded by the U.S. NSF and operated in collaboration with the Government
114 of Greenland (see Fig. 1). The station hosts a diverse array of Geoscience and Astrophysics
115 research projects (<https://www.geosummit.org/instruments>) and is the only high altitude remote
116 atmospheric observatory in the Arctic. Ambient outside air is monitored at the Temporary
117 Atmospheric Watch Observatory (TAWO), *i.e.*, ~ 1 km south of the research camp.

118 **2.1 In-situ NMHC measurements**

119 C₂-C₇ NMHCs (ethane, propane, iso-butane, n-butane, acetylene, iso-pentane, n-pentane, n-
120 hexane, benzene, toluene) were analyzed from July 2008 to July 2010 and from May 2012 to
121 March 2020 by GC-FID using a fully automated and remotely controlled custom-built system.
122 Ambient air was continuously sampled from a 10 m high inlet on the meteorological tower adjacent



123 to the TAWO building through a heated (~30°C) sampling line. The sampling frequency increased
124 from 6 ambient NMHC runs to 12 daily runs in 2018. The GC-FID system, tailored towards the
125 remote, unattended and long-term operation, is a further development of the instrument described
126 in detail by Tanner et al. (2006) and Kramer et al. (2015). The instrument relies on a cryogen-free
127 sample enrichment and injection system. Air was pulled from the tower inlet, and aliquots of the
128 sample stream were first passed through a water trap (u-shaped stainless-steel treated Silcosteel™
129 tube cooled using thermoelectric coolers) to dry the sample to a dew point of -20°C, and NMHCs
130 were then concentrated on a Peltier-cooled (-35°C) multi-stage adsorbent trap. Analysis was
131 accomplished by thermal desorption and injection onto an Al₂O₃ PLOT column for cryogen-free
132 separation on an SRI Model 8610 GC-FID. Our monitoring effort followed the World
133 Meteorological Organization (WMO) Global Atmospheric Watch (GAW) quality control
134 guidelines: blanks and calibration standards were injected every other day from the manifold and
135 processed in the exact same way as ambient samples. The limit of detection was ~2 ppt (pmol/mol
136 by volume) for all compounds and no significant blank contamination was ever noticed.
137 Quantification was based on monthly FID response factors (Scanlon and Willis, 1985) calculated
138 from the repeated analysis of two independently prepared and cross-referenced standards in use at
139 any given time. Tables S1 and S2 summarize these response factors along with the associated
140 relative standard deviation (< 5 % on average for all compounds) for 2008-2010 and 2012-2020,
141 respectively. The in-situ GC-FID system provided a stable response from 2008 to 2020, with
142 monthly response factors varying by ≤ 5 % for ethane, propane, and butanes, and by ≤ 20 % for
143 other compounds over this period. The monitoring program was audited by the World Calibration
144 Center for Volatile Organic Compounds at the site in July 2017 ([https://www.imk-ifu.kit.edu/wcc-](https://www.imk-ifu.kit.edu/wcc-voc/)
145 [voc/](https://www.imk-ifu.kit.edu/wcc-voc/)). All reported VOCs results were found to be within the Global Atmospheric Watch program
146 quality objectives (WMO, 2007).

147 **2.2 Discrete measurements**

148 We use here NMHC data from Alert, Utqiagvik, Mace Head (Ireland), Park Falls (Wisconsin,
149 USA), and Cape Kumukahi (Hawaii, USA; see Fig. 1) collected as part of the NOAA/GML CCGG
150 (October 2004 to August 2016) and HATS (August 2014 to March 2020) sampling and
151 measurement programs. Note that we combine here measurements from the two networks.

152 **2.2.1 CCGG discrete sampling and analysis**



153 As described by Steele et al. (1987) and Dlugokencky et al. (1994), air samples are collected
154 ~weekly in pairs in 2.5 L borosilicate flasks with two glass-piston stopcocks sealed with Teflon
155 O-rings. Flasks are flushed in series for 5 to 10 minutes then pressurized to ~1.2 atm with a portable
156 sampling system. Samples collected from October 2004 to August 2016 were analyzed at
157 INSTAAR in Boulder, Colorado, by GC-FID. The analysis, on a HP-5890 series II gas
158 chromatograph, first involved drying of approximately 600 cc of sample gas by running the sample
159 gas through a 6.4 mm o.d. stainless steel tube cooled to -25°C. The analytes were then
160 preconcentrated at -35°C on an adsorbent bed (Carboxen 1000/1016). Samples were thermally
161 desorbed at 310°C onto a short capillary guard column before separation on an Al₂O₃ PLOT
162 capillary column (0.53 mm × 60 m). Weekly instrument calibrations were performed using
163 primary calibration standards acquired from the NOAA Global Monitoring Laboratory, the U.K.
164 National Physics Laboratory, and the U.S. National Institute of Technology. These standards
165 scales have been maintained since 2006 by regular inter-comparison of standards from these
166 sources and propagation of the scale with newly acquired standards. Deviations in the response
167 factors from these different standards were smaller than 5 %, with results for ethane and propane
168 typically being equal or having less than 2-3 % deviation. Instrument FID response is linear within
169 the range of observed ambient concentrations. The INSTAAR NMHC laboratory was audited by
170 the WMO GAW World Calibration Center for VOCs (WCC-VOC, <https://www.imk-ifu.kit.edu/wcc-voc/>)
171 in 2008 and in 2016, and both times all measurement results passed the
172 WMO data quality criteria (WMO, 2007).

173 2.2.2 HATS discrete sampling and analysis

174 At GEOSummit, paired borosilicate glass flasks are also pressurized to ~1 atmosphere
175 overpressure with ambient air as part of the HATS sampling program. At other NH sites,
176 electropolished stainless-steel flasks are used. All flasks are analyzed by GC with mass
177 spectrometry analysis with a preconcentration system similar to Miller et al. (2008) to strip water
178 vapor and CO₂ from the airstream prior to injection of condensates (VOCs, halocarbons, solvents,
179 and other gases) onto a 0.32 mm i.d. GasPro capillary column. Results are tied to a suite of
180 standards prepared in-house with gravimetric techniques.

181 **2.3 Ancillary data**

182 Continuous monitoring of carbon monoxide (CO) has been ongoing at GEOSummit since May
183 2019 with a cavity ring-down spectroscopy (CRDS) analyzer (Picarro G-2401). A switching



184 manifold allows regular sampling of ambient air and calibration gases. Three NOAA GML
185 standards were integrated into the automated calibration. Low (69.6 ppb) and high (174.6 ppb)
186 calibration points were performed for ~3 minutes every two days, while an intermediate (117.4
187 ppb) calibration was carried out in between. Using the last minute of each calibration, the low and
188 high calibration points were used to determine the linear relationship between the certified
189 calibration values and the analyzer's reported calibration values. The calibration offset (slope and
190 intercept) was calculated and used to correct the third intermediate calibration point. The mean
191 absolute difference between the corrected and certified intermediate calibration paired values was
192 1.6 ppb, *i.e.*, 1.4 %. The minute-averaged CRDS CO ambient air data were corrected using the
193 calibration offset. The CRDS has a manufacturer-specified precision at 5 seconds, 5 minutes, and
194 60 minutes of 15, 1.5, and 1 ppb for CO (G2401 Gas Concentration Analyzer | Picarro, 2020).
195 We also use ethane, propane, tetrachloroethylene (C₂Cl₄), and hydrogen cyanide (HCN) data
196 collected in the free troposphere during the global-scale airborne Atmospheric Tomography
197 mission (ATom; <https://espo.nasa.gov/atom/content/ATom>) onboard the NASA DC-8 aircraft
198 (Wofsy et al., 2018). Canisters collected with the University of California Irvine Whole Air
199 Sampler (WAS) were analyzed for more than 50 trace gases, including ethane, propane, and
200 tetrachloroethylene by GC-FID and GC-mass spectrometric detection (Barletta et al., 2020).
201 Hydrogen cyanide was measured in situ with the California Institute of Technology Chemical
202 Ionization Mass Spectrometer (CIT-CIMS; Allen et al., 2019). For the purpose of our analysis, we
203 filtered out data collected over continents, in the marine boundary layer (altitude < 0.4 km), or
204 corresponding to stratospheric air (ozone to water vapor ratio > 1 ppb per ppm).

205 **2.4 Curve fitting method and trend analysis**

206 We used the curve fitting method developed by Thoning et al. (1989) and described in detail at
207 <https://www.esrl.noaa.gov/gmd/ccgg/mb/krvfit/krvfit.html>. Briefly, the data were fitted with a
208 function consisting of a polynomial and series of harmonics to represent the average long-term
209 trend and seasonal cycle. Residuals from the function were calculated, transformed into frequency
210 domain with a fast Fourier transform algorithm, then filtered with two low pass filters. One
211 eliminates harmonics less than ~1 month. When converted back to time domain and added to the
212 function, it gives a smoothed curve. The other filter eliminates periods less than ~1 year; when
213 transformed back to time domain and added to the polynomial, it gives the deseasonalized trend
214 (hereafter referred to as the trend). The Sen's slope estimate of the trend was calculated using



215 function TheilSen in R package openair (Carslaw and Ropkins, 2012). Note that the p-values and
216 all uncertainties are calculated through bootstrap simulations
217 (<https://davidcarslaw.github.io/openair/reference/TheilSen.html>).

218 2.5 Source apportionment analysis

219 In order to identify potential source regions, we performed a Potential Source Contribution
220 Function (PSCF) analysis using the *trajLevel* function in R package openair (Carslaw and Ropkins,
221 2012). Based on air-mass back-trajectories (see below) and NMHC residuals (see Section 2.4), the
222 PSCF calculates the probability that a source is located at latitude i and longitude j . PSCF solves:

$$223 \quad PSCF = m_{ij}/n_{ij} \quad \text{Eq.1}$$

224 where n_{ij} is the number of times that the trajectories passed through the cell (i, j) and m_{ij} the
225 number of trajectories passing through that cell in which the NMHC residual was greater than a
226 given threshold (90th percentile of the measured results distribution). Note that cells with very few
227 trajectories passing through them have a weighting factor applied to reduce their effect.

228 For each NMHC in-situ measurement, HYSPLIT (HYbrid Single Particle Lagrangian Integrated
229 Trajectory; Draxler and Rolph, 2013) 5-day air-mass back trajectories used in the PSCF analysis
230 were generated using the Python package *pysplit* (Warner, 2018) and processor *pysplitprocessor*
231 available at: <https://github.com/brendano257/pysplit> and
232 <https://github.com/brendano257/pysplitprocessor>, respectively. The HYSPLIT Lagrangian
233 particle dispersion model was run from April 2012 to June 2019 using the National Center for
234 Environmental Prediction Global Data Assimilation System (NCEP GDAS) $0.5^\circ \times 0.5^\circ$
235 meteorological inputs available at: <ftp://arlftp.arlhq.noaa.gov/pub/archives/gdas0p5>. We did not
236 generate back-trajectories for observations after June 2019 due to the unavailability of the GDAS
237 $0.5^\circ \times 0.5^\circ$ archive.

238

239 3. Results and Discussion

240 3.1 Seasonal variation

241 The seasonal variation of C₂-C₇ NMHCs at GEOSummit is displayed in Fig. 2. Summer refers to
242 June-August, fall to September-November, winter to December-February, and spring to March-
243 May. NMHCs exhibit a strong and consistent seasonal pattern year after year, with maximum mole
244 fractions during winter and early spring, and a rapid decline towards summer. Anthropogenic
245 sources of NMHCs do not vary much seasonally (Pozzer et al., 2010). Therefore, the observed



246 seasonal cycle is primarily driven by the seasonally changing sink strength by the photochemically
247 formed OH radical (Goldstein et al., 1995) – the dominant oxidizing agent in the global
248 troposphere (Levy, 1971; Logan et al., 1981; Thompson, 1992). We found a significant correlation
249 ($R^2 = 0.7$, p -value < 0.001) between the mean seasonal amplitude of individual NMHCs and their
250 lifetime against oxidation by the OH radical (Fig. S1). During the summer period, mole fractions
251 of the heavier NMHCs were below or close to the GEOSummit in-situ system detection limit (Fig.
252 2b). As already noted by Goldstein et al. (1995) and Kramer et al. (2015) based on a limited dataset,
253 the phase of each NMHC is shifted due to the rate of reaction with OH. Ethane, the lightest and
254 longest lived of the NMHCs shown in Fig. 2, peaks in February/March with a median of 2110 ppt,
255 and declines to a minimum of 734 ppt in July. Heavier and shorter-lived NMHCs have lower mole
256 fractions, peak earlier in the year (January/February), and reach a minimum earlier in summer
257 (June) due to their faster rate of reaction with OH (Chameides and Cicerone, 1978).
258 Because changes in NMHC sources and sinks can affect the seasonal cycle amplitude, we
259 investigated whether there is a trend in the NMHC's amplitude at GEOSummit. We focus here on
260 ethane and propane, the most abundant hydrocarbons in the remote atmosphere after methane.
261 Figure 3 shows the amplitude of the ethane and propane seasonal cycles, determined as the relative
262 difference between the maximum and minimum values from the smooth curve for each annual
263 cycle (Dlugokencky et al., 1997). The peak-to-minimum relative amplitude ranged from 64 to 71
264 % for ethane and from 92 to 96 % for propane, and there is no indication of a significant overall
265 trend in amplitude. This range of amplitudes is in good agreement with the literature: the typical
266 seasonal amplitudes for ethane are on the order of 50 % at mid-latitude sites and can increase up
267 to 80 % at remote sites (Franco et al., 2016; Helmig et al., 2016). Changes in mole fractions are
268 further investigated and discussed in the following section.

269 **3.2 Reversal of ethane and propane rates of change at GEOSummit in 2015**

270 Ethane is released from seepage of fossil carbon deposits, volcanoes, fires, and from human
271 activities – with O&NG extraction, processing, distribution, and industrial use being the primary
272 sources (Poizzer et al., 2010). Based on the inventory developed for the Hemispheric Transport of
273 Air Pollutants, Phase II (HTAP2, Janssens-Maenhout et al., 2015), biogenic emissions from
274 MEGAN2.1 (Guenther et al., 2012), and fire emissions from FINNv1.5 (Wiedinmyer et al., 2011),
275 Helmig et al. (2016) estimated that ~4 %, 18 %, and 78 % of global ethane emissions are due to
276 biogenic, biomass burning, and anthropogenic sources, respectively. Global ethane emission rates



277 decreased by 21 % from 1984 to 2010 likely due to decreased venting and flaring of natural gas in
278 oil producing fields (Simpson et al., 2012). As a consequence, atmospheric ethane background air
279 mixing ratios significantly declined during 1984-2010, by an average of -12.4 ± 1.3 ppt per year
280 in the Northern Hemisphere. However, the analysis of ten years (2004-2014) of NMHC data from
281 air samples collected at NOAA GML remote global sampling sites (including GEOSummit)
282 showed a reversal of the global ethane trend from mid-2009 to mid-2014 (ethane growth rates $>$
283 50 ppt per year at 32 sites). This trend reversal was attributed to increased U.S. O&NG production
284 (Helmig et al., 2016). Figure 4a shows the July 2008-March 2020 ethane trend at GEOSummit, as
285 inferred from our in-situ measurements. Note that the same time-series but also showing individual
286 data points can be found in Fig. S2. Ethane mixing ratios at GEOSummit significantly (p-value $<$
287 0.001) increased by $+69.0$ [$+47.4, +73.2$; 95 % confidence interval] ppt per year from January
288 2010 to December 2014. A reversal is, however, evident after 2015: ethane mixing ratios
289 significantly (p-value $<$ 0.001) decreased by -58.4 [$-64.1, -48.9$] ppt per year from January 2015
290 to December 2018. Data collected after 2019, however, suggest that the pause in the growth of
291 atmospheric ethane might only be temporary. We focus hereafter on the year 2015 reversal. Similar
292 to ethane, a reversal is evident late 2014 for propane (see Fig. 4b): mixing ratios significantly (p-
293 value $<$ 0.001) increased by $+47.9$ [$+32.3, +52.3$] ppt per year from January 2010 to June 2014,
294 but significantly (p-value $<$ 0.001) decreased at a rate of -70.5 [$-76.1, -65.8$] ppt per year from July
295 2014 to July 2016. Propane mixing ratios remained fairly stable ($+10.2$ [$+6.6, +14.6$] ppt per year;
296 p-value $<$ 0.001) from July 2016 to December 2019. It should be noted that the pause in the growth
297 of atmospheric ethane and propane at GEOSummit in 2015-2018 is confirmed by independent
298 discrete sampling under the umbrella of the NOAA/GML CCGG and HATS networks (see Fig. 4;
299 solid lines). Figure S3 shows the good agreement ($R^2 = 0.97$ for ethane, $R^2 = 0.99$ for propane)
300 between in-situ GC-FID measurements and discrete samples.

301 The temporary pause in the growth of ethane and propane at GEOSummit could either suggest a
302 change in: i) the OH sink strength, ii) atmospheric transport from source regions and/or iii)
303 natural/anthropogenic emissions.

304 The tropospheric abundance of OH is driven by a complex series of chemical reactions involving
305 tropospheric ozone, methane, carbon monoxide, NMHCs, and nitrogen oxides, and by the levels
306 of solar radiation and humidity (Logan et al., 1981; Thompson, 1992). Building on the comparison
307 of modeled and observed methane and methyl chloroform lifetimes, Naik et al. (2013) showed that



308 OH concentrations changed little from 1850 to 2000. The authors suggested that the increases in
309 factors that enhance OH (humidity, tropospheric ozone, nitrogen oxide emissions, and UV
310 radiation) was compensated by increases in OH sinks (methane abundance, carbon monoxide and
311 NMHC emissions). More recently, Naus et al. (2020) used a 3D-model inversion of methyl
312 chloroform to constrain the atmospheric oxidative capacity – largely determined by variations in
313 OH – for the period 1998-2018. The authors showed that the interannual variations were typically
314 small (<3 % per year) and found no evidence of a significant long-term trend in OH over the study
315 period. Changes in NMHC mole fractions at GEOSummit are well outside what could be explained
316 by a 3% change in OH tropospheric concentrations. There is, however, likely a difference between
317 global and regional OH variations (Brenninkmeijer et al., 1992; Spivakovsky et al., 2000;
318 Lelieveld et al., 2004). In the absence of data on the Arctic and mid-latitudes OH abundance, we
319 concede that OH may play a role on the observed pause but do not discuss that hypothesis further.
320 The latter two hypotheses are investigated and verified or rejected in the following sections.

321 **3.3 No evidence for a change in transport from source regions**

322 The synoptic-scale tropospheric circulation in the Arctic is driven by three major semi-permanent
323 pressure systems: i) the Aleutian Low, low-pressure center located south of the Bering Sea area,
324 ii) the Icelandic Low, low-pressure system located southeast of Greenland near Iceland, and iii)
325 the Siberian High, high-pressure center located over eastern Siberia (Barrie et al., 1992). During
326 positive phases of the North Atlantic Oscillation (NAO), the Icelandic Low is strengthened and
327 transport into the Arctic enhanced, resulting in higher Arctic pollution levels (Duncan and Bey,
328 2004; Eckhardt et al., 2003). Negative phases of the NAO are associated with decreased transport
329 from Europe and Siberia and increased transport from North America. In addition, mid-latitude
330 atmospheric blocking events – quasi-stationary features characterized by a high-pressure cell
331 centered around 60°N and lasting up to ~15 days (Rex, 1950) – are known to enhance transport of
332 polluted air to the Arctic (Iversen and Joranger, 1985). Here, we test the hypothesis of a pause in
333 the growth of atmospheric ethane and propane at GEOSummit driven by the interannual variability
334 of pollution transport from source regions.

335 The interannual variability in the origin of air masses influencing GEOSummit was investigated
336 using April 2012-June 2019 air-mass back trajectories generated with the HYSPLIT model. Figure
337 5 shows the annual gridded back trajectory frequencies and Figure 6a summarizes the relative
338 contribution of each geographical sector for each year. Contrary to other Arctic sites (Hirdman et



339 al., 2010), GEOSummit is mostly influenced by transport from North America and Europe,
340 whereas Siberia has relatively little influence (0-2 %). European air masses represented 3-6 % of
341 the total, with a 10 % high in 2018. The relative contribution of North Atlantic air masses (“ocean”)
342 ranged from 1 to 9 %, with a 14 % high from January to August 2019. The frequency of North
343 American air masses exhibited the most variability, ranging from 2 to 20 %. Assuming that the
344 ethane and propane trends are driven by emissions in North America (Helmig et al., 2016) and that
345 these emissions are constant, one would expect higher ethane and propane mixing ratios in years
346 when the relative influence of North American air masses peaked. There is, however, an
347 anticorrelation: a 2-3 % relative contribution of North American air masses in 2014 and 2015 when
348 ethane/propane mixing ratios reached a maximum, and 19 % in 2018 when mixing ratios reached
349 a minimum. This leaves two possibilities: either North American emissions dropped over the
350 studied time period (see Section 3.4), or ethane/propane trends observed at GEOSummit are not
351 driven by emissions in North America (see below).

352 Local/regional air masses (*i.e.*, around Greenland, see Fig. 5) were the most frequently impacting
353 the site (located near the receptor site). Interestingly, their relative contribution increased from 79
354 % in 2012 to 91-93 % in 2014-2015 before gradually dropping to 61 % in 2018. The apparent
355 correlation between the relative contribution of local/regional air masses and the ethane/propane
356 trend raises the question of whether these are connected. In order to identify potential sources in
357 this sector, we performed a PSCF analysis to investigate source-receptor relationships (e.g.,
358 Pekney et al., 2006; Perrone et al., 2018; Yu et al., 2015; Zhou et al., 2018; Zong et al., 2018). The
359 PSCF calculates the probability that a source is located at latitude i and longitude j (Pekney et al.,
360 2006). Figure S4 shows the results of the PSCF analysis for ethane and propane residuals and
361 shows no consistent pattern associated with elevated concentrations. In both winter and summer,
362 the probability of an ethane or propane source from this analysis is low (<2 % on average).

363 The history of petroleum exploration activities on the Greenland continental shelf dates back to
364 the 1970s (Arctic Oil & Gas Development: The Case of Greenland, 2020). More recently, the
365 Greenland’s government announced the opening of three new offshore areas for exploration in
366 November 2020 (Greenland Opens Offshore Areas for Drilling, 2020). Despite exploration drilling
367 activities, there has never been any O&NG exploitation of Greenland resources (Arctic Oil &
368 Gas Development: The Case of Greenland, 2020). Building on the above, the assumption of a
369 significant local/regional source can be ruled out, and so can the hypothesis that the pause in the



370 growth of ethane and propane is driven by local/regional emissions. The last remaining hypothesis
371 is that this pause is due to a change in emissions from any of the other source sectors, or a
372 combination of them, or total NH emissions and associated change in baseline NH atmospheric
373 levels. This hypothesis is tested in the following Section using observations at other baseline sites.

374 **3.4 Evidence for a hemispheric pattern**

375 Table 1 summarizes the rate of change and 95 % confidence interval for 2010-2014 and 2015-
376 2018 at Alert (ALT, Nunavut, Canada), Utqiagvik/Barrow (BRW, Alaska, USA), Cape Kumukahi
377 (KUM, Hawaii, USA), Park Falls (LEF, Wisconsin, USA), and Mace Head (MHD, Ireland – see
378 Fig. 1) where discrete samples were collected for the NOAA/GML CCGG and HATS cooperative
379 networks. A clear reversal in interannual changes for ethane and propane mixing ratios is observed
380 in 2015 at ALT, BRW, KUM, and LEF. These results support the observed changes at
381 GEOSummit and indicate a hemispheric pattern, likely due to a change in Northern Hemisphere
382 emissions, with a turning point around late 2014. Biomass burning and anthropogenic activities
383 being the main emitters of NMHCs, we hereafter focus the discussion on these two sources.

384 **3.4.1 Biomass burning**

385 Occasional biomass burning plumes were observed at GEOSummit. For example, Fig. 7 shows
386 the simultaneous increase in CO, ethane, propane, and benzene mixing ratios for a short number
387 of days in July and August 2019. According to the Whole Atmosphere Community Climate Model
388 (WACCM; Gettelman et al., 2019) CO forecast simulations, available at
389 <https://www.acom.ucar.edu/waccm/forecast/>, these enhancements can be attributed to intense
390 Siberian wildfires occurring at that time (Bondur et al., 2020). In good agreement with the
391 WACCM simulations, emission ratios (amount of compound emitted divided by that of a reference
392 compound) derived from these two plumes for ethane and propane ($5.4\text{-}5.9 \times 10^{-3}$ and $1.5\text{-}1.6$
393 $\times 10^{-3}$ ppb per ppb of CO, respectively; see Fig. S5) are within the range of values reported for
394 boreal forest and peat fires (Andreae, 2019).

395 Despite the observation of occasional plumes at GEOSummit, the question remains whether
396 biomass burning could drive the observed hemispheric pause in the growth of atmospheric ethane
397 and propane. Figure 6b gives annual biomass burning emissions from all open burning north of
398 45°N according to the Fire INventory from NCAR (FINNv2.2) emission estimates driven by
399 MODIS fire detections (Wiedinmyer et al., in prep). Emissions peaked in 2012, known for being
400 an exceptional wildfire season in the contiguous U.S. (e.g., Lassman et al., 2017; Val Martin et al.,



401 2013). While propane emissions remained fairly stable from 2014 to 2018, ethane emissions
402 slightly decreased from 2014 to 2016. However, we did not find any correlation between annual
403 biomass burning emissions and annually-averaged mixing ratios (true using either 2009-2018 or
404 2015-2018 data). The seasonal analysis of the correlation between ambient air mixing ratios and
405 biomass burning emissions yielded similar results. This suggests that the observed pause in the
406 growth of atmospheric ethane and propane is likely not driven by biomass burning emissions.
407 This conclusion is further supported by measurements during the global-scale aircraft mission
408 ATom. Using ethane and propane data collected in the Northern Hemisphere ($>20^{\circ}\text{N}$) remote free
409 troposphere during the four ATom seasonal deployments, we found a significant positive
410 correlation of ethane and propane with tetrachloroethylene ($R^2 = 0.6$, $p\text{-value} < 0.001$) and a poor
411 correlation with hydrogen cyanide ($R^2 < 0.1$, $p\text{-value} < 0.001$; see Fig. S6), used as tracers of
412 anthropogenic and biomass burning emissions, respectively (Bourgeois et al., in prep.). These
413 results from the remote free troposphere confirm that atmospheric ethane and propane ambient air
414 levels are mostly driven by anthropogenic activities rather than by biomass burning emissions, in
415 line with results from other studies (e.g., Xiao et al., 2008).

416 3.4.2 O&NG activities

417 Discrete samples collected at northern-hemisphere baseline sites show that the strongest change
418 was observed at LEF, located downwind from the Bakken oil field in North Dakota (Gvakharia et
419 al., 2017), with an increase of ethane mixing ratios of +167.7 [+157.5, +186.0] ppt per year in
420 2010-2014 and a decrease of -247.8 [-312.2, -158.2] ppt per year in 2015-2018 (see Table 1). This
421 result, along with previous findings by Helmig et al. (2016) and Franco et al. (2015), supports the
422 hypothesis that U.S. O&NG emissions could play a major role in driving atmospheric ethane and
423 propane concentrations in the NH. Here we further discuss this potential contribution to the
424 observed hemispheric pause in the growth of atmospheric ethane and propane in 2015-2018.

425 The U.S. has experienced dramatic increases in O&NG production since 2005, underpinned by
426 technological developments such as horizontal drilling and hydraulic fracturing (Caporin and
427 Fontini, 2017; Feng et al., 2019). This shale revolution has transformed the U.S. into the world's
428 top O&NG producer (Gong, 2020). Coincident with the shale gas boom, the U.S. production of
429 natural gas liquids (ethane, propane, butane, iso-butane, and pentane) has significantly increased
430 in the past decade from 0.6-0.7 billion barrels in the 2000s to 1.1 billion barrels in 2014, and close
431 to 1.8 billion barrels in 2019 (U.S. Field Production of Natural Gas Liquids, 2021). Ethane and



432 propane emissions are primarily due to leakage during the production, processing, and
433 transportation of natural gas (Tzompa-Sosa et al., 2019; Pétron et al., 2012).

434 Propane is extracted from natural gas stream and used as a heating fuel. As shown in Figure 8, the
435 U.S. propane field production temporarily plateaued from June 2014 to December 2016 (U.S. Field
436 Production of Propane, 2021) due to a slowdown in natural gas production in response to low
437 natural gas prices. As we consider recent changes in emissions, however, changes in emissions per
438 unit of production must also be considered. A recent study in the Northeastern Colorado Denver-
439 Julesburg Basin showed little change in atmospheric hydrocarbons, including propane, in 2008-
440 2016 despite a 7-fold increase in oil production and nearly tripling of natural gas production,
441 suggesting a significant decrease in leak and/or venting rate per unit of production (Oltmans et al.,
442 in review). While we cannot reliably estimate how propane emissions might have changed during
443 this recent period, these two influences, combined together, could explain the observed temporary
444 pause in the growth of atmospheric propane.

445 Estimating the total production, and ultimately emissions, of ethane is even more complex as it
446 depends on the ethane-to-natural gas price differential. Ethane has long been considered an
447 unwanted byproduct of O&NG drilling, much of it burned away in the natural gas stream or flared
448 off at well sites. Today, ethane is a key feedstock for petrochemical manufacturing and the U.S. is
449 currently the top producer and exporter of ethane (Sicotte, 2020). Depending on the price of ethane
450 relative to natural gas, ethane can be left in the natural gas stream and sold along with natural gas
451 – a process known as ethane rejection, or separated at natural gas processing plants along with
452 other natural gas liquids (such as propane). Assuming the same leak rates for ethane as for methane,
453 85 % of ethane emissions are due to natural gas extraction and processing, while processed natural
454 gas transportation and use only represent 15 % of the natural gas supply chain ethane loss rate
455 (Alvarez et al., 2018). The slowdown in natural gas production from June 2014 to December 2016
456 (see above) may thus have contributed to the atmospheric ethane plateauing. However, these
457 estimates do not take into account emissions of ethane from its own supply chain (e.g., separation,
458 storage, liquefaction for export, ethane cracker to produce ethylene and plastic resins) – for which
459 leak rates remain unknown. A number of top-down studies, focusing on specific regions or time-
460 periods (e.g., 2010-2014), have shown that current inventories underestimate ethane emissions
461 (e.g., Tzompa-Sosa et al., 2017; Pétron et al., 2014). The modeling study led by Dalsøren et al.
462 (2018) focusing on year 2011 showed that fossil fuel emissions of ethane are likely biased-low by



463 a factor of 2-3. In this highly dynamic context, where ethane production and volume rejected
464 continuously vary and where leak rates change over time (Schwietzke et al., 2014), there is a need
465 for further hemispheric- or global-scale top-down studies focusing on the interannual variability
466 of ethane emissions.

467

468 **4. Summary and Conclusion**

469 Ethane and propane are the most abundant atmospheric NMHCs and they exert a strong influence
470 on tropospheric ozone, a major air pollutant and greenhouse gas. Increasing levels have been
471 reported in the literature from 2009 to 2014, with evidence pointing at U.S. O&NG activities as
472 the most likely cause (Kort et al., 2016; Helmig et al., 2016; Franco et al., 2016; Hausmann et al.,
473 2016). The long-term high-resolution records of ambient air C₂-C₇ NMHCs at GEOSummit
474 presented here confirm that atmospheric ethane and propane levels increased in the remote arctic
475 troposphere from 2009 to 2015, but also reveal a pause in their growth in 2015-2018. The analysis
476 of air-mass back-trajectories allowed us to rule out the possibility that this pause is driven by a
477 change in transport from source regions. Using independent discrete samples collected at other
478 NH baseline sites, we show that this pause is observed throughout the northern hemisphere –
479 suggesting a change in total NH emissions and in baseline NH atmospheric levels. We further
480 investigated and discussed the contribution of the two main NMHC emitters: biomass burning and
481 O&NG production. We did not find any correlation between atmospheric ethane and propane
482 mixing ratios and the FINNv2.2 biomass burning emission estimates. Additionally, data collected
483 in the NH remote free troposphere during the ATom aircraft campaign support that atmospheric
484 ethane and propane ambient air levels are mostly driven by anthropogenic activities rather than by
485 biomass burning emissions. The fact that the strongest rate of change reversal was observed at a
486 site located downwind from the Bakken oil field in North Dakota tends to suggest that U.S. O&NG
487 activities yet again played a major role here. The slowdown in U.S. natural gas production from
488 June 2014 to December 2016 combined with a decrease in leak rate per unit of production could
489 have contributed to the observed temporary pause. This conclusion is, however, tentative given
490 the large uncertainties associated with emission estimates, especially with ethane emissions from
491 its supply chain. We hope this work can be used as a starting point to understand what led to the
492 pause in the growth of atmospheric ethane and propane in 2015-2018 and, more generally, to what



493 extent ON&G activities could be responsible for variations in NH baseline ethane and propane
494 levels.

495

496 **Data availability**

497 All non-methane hydrocarbons and carbon monoxide in-situ data used in this study are archived
498 and publicly available on the Arctic Data Center database (Angot et al., 2020; Helmig, 2017).
499 NOAA/GML HATS and CCGG discrete data are available at
500 <ftp://aftp.cmdl.noaa.gov/data/hats/PERSEUS> and ftp://aftp.cmdl.noaa.gov/data/trace_gases/voc/,
501 respectively.

502

503 **Author contribution**

504 DH initiated the long-term monitoring effort at GEOSummit and secured funding over the years.
505 JH designed and built the GC-FID used for NMHC in-situ monitoring and performed ~bi-annual
506 on-site visits for maintenance and calibration operations. CD, JC, and BB performed the in-situ
507 data processing (*i.e.*, GC peak identification, peak integration, background subtraction, and
508 calculation of mixing ratios). CD, JC, and HA analyzed the data under the supervision of CW and
509 DH. GP helped evaluating the impact ON&G activities on NMHC trends while IB and CW helped
510 evaluating the impact of biomass burning. IV, SAM, BRM and JWE provided the NOAA /GML
511 HATS discrete data. JH and DH provided the NOAA/GML CCGG NMHC discrete data with
512 contribution from CD, JC, and BB. HA wrote the manuscript with contribution from all co-authors.

513

514 **Competing interests**

515 The authors declare no competing interests.

516

517 **Acknowledgements**

518 We would like to thank the GEOSummit Science Technicians and CH2MHill Polar Services for
519 their tremendous support in enabling on-site and flask collections at the station. HA, JH, and DH
520 would like to acknowledge Maria Soledad Pazos, Miguel Orta Sanchez, and all students involved
521 in the NMHC flask analysis at INSTAAR. IV, SAM, and BRM thank the instrumental analysis
522 assistance of C. Siso and M. Crotwell and standards prepared and maintained by B. Hall at the



523 NOAA GML. We would also like to thank Donald Blake, Paul Wennberg, Michelle Kim, Hannah
524 Allen, John Crouse, and Alex Teng for the ATom dataset used in this analysis.

525

526 **Financial support**

527 The long-term observations and analysis efforts were supported by the National Science
528 Foundation (grant nos. 1108391 and 1822406) and the NASA ROSES program (grant no.
529 NNX07AR26G). Undergraduate students Connor Davel and Jashan Chopra received financial
530 support from the University of Colorado Boulder's Undergraduate Research Opportunities
531 Program (UROP; grant nos. 7245334 and 5269631, respectively). Support for most CIRES
532 employees is from NOAA award no. NA17OAR4320101. ATom was funded by NASA ROSES-
533 2013 NRA NNH13ZDA001N-EVS2.

534

535 **References**

536 Allen, H. M., Crouse, J. D., Kim, M. J., Teng, A. P., and Wennberg, P. O.: Atmospheric Tomography Mission
537 (ATom) ATom: L2 In Situ Data from Caltech Chemical Ionization Mass Spectrometer (CIT-CIMS), 79.481444 MB,
538 <https://doi.org/10.3334/ORNLDAAAC/1713>, 2019.

539 Alvarez, R. A., Zavala-Araiza, D., Lyon, D. R., Allen, D. T., Barkley, Z. R., Brandt, A. R., Davis, K. J., Herndon, S.
540 C., Jacob, D. J., Karion, A., Kort, E. A., Lamb, B. K., Lauvaux, T., Maasakkers, J. D., Marchese, A. J., Omara, M.,
541 Pacala, S. W., Peischl, J., Robinson, A. L., Shepson, P. B., Sweeney, C., Townsend-Small, A., Wofsy, S. C., and
542 Hamburg, S. P.: Assessment of methane emissions from the U.S. oil and gas supply chain, 361, 186–188,
543 <https://doi.org/10.1126/science.aar7204>, 2018.

544 Andreae, M. O.: Emission of trace gases and aerosols from biomass burning – an updated assessment, 19, 8523–8546,
545 <https://doi.org/10.5194/acp-19-8523-2019>, 2019.

546 Angot, H., Helmig, D., Hueber, J., Chopra, J., Davel, C., and Wiedinmyer, C.: Atmospheric tracers for Arctic wildfires,
547 air pollution, atmospheric chemistry, and climate change at GEOSummit, Greenland, since 2018,
548 <https://doi.org/10.18739/A2FX73Z7B>, 2020.

549 Aydin, M., Verhulst, K. R., Saltzman, E. S., Battle, M. O., Montzka, S. A., Blake, D. R., Tang, Q., and Prather, M. J.:
550 Recent decreases in fossil-fuel emissions of ethane and methane derived from firm air, *Nature*, 476, 198–201,
551 <https://doi.org/10.1038/nature10352>, 2011.

552 Barletta, B., Biggs, B. C., Blake, D. R., Blake, N., Hoffman, A., Hughes, S., Meinardi, S., Vizenor, N., and Woods,
553 C. T.: ATom: L2 Halocarbons and Hydrocarbons from the UC-Irvine Whole Air Sampler (WAS),
554 <https://doi.org/10.3334/ORNLDAAAC/1751>, 2020.

555 Barrie, L. A., Gregor, D., Hargrave, B., Lake, R., Muir, D., Shearer, R., Tracey, B., and Bidleman, T.: Arctic
556 contaminants: sources, occurrence and pathways, *Science of The Total Environment*, 122, 1–74,
557 [https://doi.org/10.1016/0048-9697\(92\)90245-N](https://doi.org/10.1016/0048-9697(92)90245-N), 1992.

558 Bondur, V. G., Mikhov, I. I., Voronova, O. S., and Sitnov, S. A.: Satellite Monitoring of Siberian Wildfires and Their
559 Effects: Features of 2019 Anomalies and Trends of 20-Year Changes, *Dokl. Earth Sc.*, 492, 370–375,
560 <https://doi.org/10.1134/S1028334X20050049>, 2020.



- 561 Bourgeois, I., Peischl, J., Neuman, A., Brown, S., Thompson, C., Angot, H., Apel, E., Baublitz, C., Brewer, J.,
562 Commane, R., Daube, B., Diskin, G. W., Emmons, L., Fischer, E. V., Fiore, A. M., Gkatzelis, G., Hills, A., Hornbrook,
563 R. S., Lacey, F., Murray, L., Wofsy, S. C., and Ryerson, T. B.: Biomass burning emissions drive ozone enhancements
564 in the global remote troposphere, in prep.
- 565 Brenninkmeijer, C. A. M., Manning, M. R., Lowe, D. C., Wallace, G., Sparks, R. J., and Volz-Thomas, A.:
566 Interhemispheric asymmetry in OH abundance inferred from measurements of atmospheric 14 CO, 356, 50–52,
567 <https://doi.org/10.1038/356050a0>, 1992.
- 568 Caporin, M. and Fontini, F.: The long-run oil–natural gas price relationship and the shale gas revolution, *Energy*
569 *Economics*, 64, 511–519, <https://doi.org/10.1016/j.eneco.2016.07.024>, 2017.
- 570 Carslaw, D. and Ropkins, K.: openair - An R package for air quality data analysis, *Environ Modell Softw*, 27–28, 52–
571 61, <https://doi.org/10.1016/j.envsoft.2011.09.008>, 2012.
- 572 Chameides, W. L. and Cicerone, R. J.: EFFECTS OF NONMETHANE HYDROCARBONS IN THE
573 ATMOSPHERE., 83, 947–952, <https://doi.org/10.1029/JC083iC02p00947>, 1978.
- 574 Dalsøren, S. B., Myhre, G., Hodnebrog, Ø., Myhre, C. L., Stohl, A., Pisso, I., Schwietzke, S., Höglund-Isaksson, L.,
575 Helmig, D., Reimann, S., Sauvage, S., Schmidbauer, N., Read, K. A., Carpenter, L. J., Lewis, A. C., Punjabi, S., and
576 Wallasch, M.: Discrepancy between simulated and observed ethane and propane levels explained by underestimated
577 fossil emissions, 11, 178–184, <https://doi.org/10.1038/s41561-018-0073-0>, 2018.
- 578 Dlugokencky, E. J., Steele, L. P., Lang, P. M., and Masarie, K. A.: The growth rate and distribution of atmospheric
579 methane, 99, 17021–17043, <https://doi.org/10.1029/94JD01245>, 1994.
- 580 Dlugokencky, E. J., Masarie, K. A., Tans, P. P., Conway, T. J., and Xiong, X.: Is the amplitude of the methane seasonal
581 cycle changing?, *Atmospheric Environment*, 31, 21–26, [https://doi.org/10.1016/S1352-2310\(96\)00174-4](https://doi.org/10.1016/S1352-2310(96)00174-4), 1997.
- 582 Draxler, R. R. and Rolph, G. D.: HYSPLIT (HYbrid Single-Particle Lagrangian Integrated Trajectory) Model access
583 via NOAA ARL READY Website (<http://www.arl.noaa.gov/HYSPLIT.php>), last access: 24 October 2015. NOAA
584 Air Resources Laboratory, College Park, MD., 2013.
- 585 Duncan, B. N. and Bey, I.: A modeling study of the export pathways of pollution from Europe: Seasonal and
586 interannual variations (1987-1997), 109, D08301, <https://doi.org/10.1029/2003JD004079>, 2004.
- 587 Eckhardt, S., Stohl, A., Beirle, S., Spichtinger, N., James, P., Forster, C., Junker, C., Wagner, T., Platt, U., and
588 Jennings, S. G.: The North Atlantic Oscillation controls air pollution transport to the Arctic, 3, 1769–1778,
589 <https://doi.org/10.5194/acp-3-1769-2003>, 2003.
- 590 Feng, G.-F., Wang, Q.-J., Chu, Y., Wen, J., and Chang, C.-P.: Does the shale gas boom change the natural gas price-
591 production relationship? Evidence from the U.S. market, *Energy Economics*, 104327,
592 <https://doi.org/10.1016/j.eneco.2019.03.001>, 2019.
- 593 Franco, B., Bader, W., Toon, G. C., Bray, C., Perrin, A., Fischer, E. V., Sudo, K., Boone, C. D., Bovy, B., Lejeune,
594 B., Servais, C., and Mahieu, E.: Retrieval of ethane from ground-based FTIR solar spectra using improved
595 spectroscopy: Recent burden increase above Jungfrauoch, *Journal of Quantitative Spectroscopy and Radiative*
596 *Transfer*, 160, 36–49, <https://doi.org/10.1016/j.jqsrt.2015.03.017>, 2015.
- 597 Franco, B., Mahieu, E., Emmons, L. K., Tzompa-Sosa, Z. A., Fischer, E. V., Sudo, K., Bovy, B., Conway, S., Griffin,
598 D., Hannigan, J. W., Strong, K., and Walker, K. A.: Evaluating ethane and methane emissions associated with the
599 development of oil and natural gas extraction in North America, *Environ. Res. Lett.*, 11, 044010,
600 <https://doi.org/10.1088/1748-9326/11/4/044010>, 2016.



- 601 Geller, L. S., Elkins, J. W., Lobert, J. M., Clarke, A. D., Hurst, D. F., Butler, J. H., and Myers, R. C.: Tropospheric
602 SF6: Observed latitudinal distribution and trends, derived emissions and interhemispheric exchange time, 24, 675–
603 678, <https://doi.org/10.1029/97GL00523>, 1997.
- 604 Gettelman, A., Mills, M. J., Kinnison, D. E., Garcia, R. R., Smith, A. K., Marsh, D. R., Tilmes, S., Vitt, F., Bardeen,
605 C. G., McInerney, J., Liu, H.-L., Solomon, S. C., Polvani, L. M., Emmons, L. K., Lamarque, J.-F., Richter, J. H.,
606 Glanville, A. S., Bacmeister, J. T., Phillips, A. S., Neale, R. B., Simpson, I. R., DuVivier, A. K., Hodzic, A., and
607 Randel, W. J.: The Whole Atmosphere Community Climate Model Version 6 (WACCM6), 124, 12380–12403,
608 <https://doi.org/10.1029/2019JD030943>, 2019.
- 609 Goldstein, A. H., Wofsy, S. C., and Spivakovsky, C. M.: Seasonal variations of nonmethane hydrocarbons in rural
610 New England: Constraints on OH concentrations in northern midlatitudes, 100, 21023–21033,
611 <https://doi.org/10.1029/95JD02034>, 1995.
- 612 Gong, B.: The Development and Implication of Nature Gas Market in the Context of the Shale Revolution, in: Shale
613 Energy Revolution: The Rise and Fall of Global Oil and Gas Industry, edited by: Gong, B., Springer, Singapore, 19–
614 36, https://doi.org/10.1007/978-981-15-4855-0_2, 2020.
- 615 Guenther, A. B., Jiang, X., Heald, C. L., Sakulyanontvittaya, T., Duhl, T., Emmons, L. K., and Wang, X.: The Model
616 of Emissions of Gases and Aerosols from Nature version 2.1 (MEGAN2.1): an extended and updated framework for
617 modeling biogenic emissions, 5, 1471–1492, <https://doi.org/10.5194/gmd-5-1471-2012>, 2012.
- 618 Gvakharia, A., Kort, E. A., Brandt, A., Peischl, J., Ryerson, T. B., Schwarz, J. P., Smith, M. L., and Sweeney, C.:
619 Methane, Black Carbon, and Ethane Emissions from Natural Gas Flares in the Bakken Shale, North Dakota, Environ.
620 Sci. Technol., 51, 5317–5325, <https://doi.org/10.1021/acs.est.6b05183>, 2017.
- 621 Hartery, S., Commane, R., Lindaas, J., Sweeney, C., Henderson, J., Mountain, M., Steiner, N., McDonald, K., Dinardo,
622 S. J., Miller, C. E., Wofsy, S. C., and Chang, R. Y.-W.: Estimating regional-scale methane flux and budgets using
623 CARVE aircraft measurements over Alaska, 18, 185–202, <https://doi.org/10.5194/acp-18-185-2018>, 2018.
- 624 Hausmann, P., Sussmann, R., and Smale, D.: Contribution of oil and natural gas production to renewed increase in
625 atmospheric methane (2007–2014): top–down estimate from ethane and methane column observations, 16, 3227–
626 3244, <https://doi.org/10.5194/acp-16-3227-2016>, 2016.
- 627 Helmig, D.: Atmospheric hydrocarbons as tracers for climate change, air transport, and oxidation chemistry in the
628 Arctic, GEOSummit, Greenland, 2008-2017., <https://doi.org/10.18739/A2RS0X>, 2017.
- 629 Helmig, D., Bottenheim, J., Galbally, I. E., Lewis, A., Milton, M. J. T., Penkett, S., Plass-Duelmer, C., Reimann, S.,
630 Tans, P., and Thiel, S.: Volatile Organic Compounds in the Global Atmosphere, 90, 513–514,
631 <https://doi.org/10.1029/2009EO520001>, 2009.
- 632 Helmig, D., Petrenko, V., Martinerie, P., Witrant, E., Röckmann, T., Zuiderweg, A., Holzinger, R., Hueber, J.,
633 Thompson, C., White, J. W. C., Sturges, W., Baker, A., Blunier, T., Etheridge, D., Rubino, M., and Tans, P.:
634 Reconstruction of Northern Hemisphere 1950-2010 atmospheric non-methane hydrocarbons, 14, 1463–1483,
635 <https://doi.org/10.5194/acp-14-1463-2014>, 2014.
- 636 Helmig, D., Rossabi, S., Hueber, J., Tans, P., Montzka, S. A., Masarie, K., Thoning, K., Plass-Duelmer, C., Claude,
637 A., Carpenter, L. J., Lewis, A. C., Punjabi, S., Reimann, S., Vollmer, M. K., Steinbrecher, R., Hannigan, J. W.,
638 Emmons, L. K., Mahieu, E., Franco, B., Smale, D., and Pozzer, A.: Reversal of global atmospheric ethane and propane
639 trends largely due to US oil and natural gas production, 9, 490–495, <https://doi.org/10.1038/ngeo2721>, 2016.
- 640 Hirdman, D., Sodemann, H., Eckhardt, S., Burkhart, J. F., Jefferson, A., Mefford, T., Quinn, P. K., Sharma, S., Ström,
641 J., and Stohl, A.: Source identification of short-lived air pollutants in the Arctic using statistical analysis of
642 measurement data and particle dispersion model output, 10, 669–693, <https://doi.org/10.5194/acp-10-669-2010>, 2010.



- 643 Houweling, S., Dentener, F., and Lelieveld, J.: The impact of nonmethane hydrocarbon compounds on tropospheric
644 photochemistry, 103, 10673–10696, <https://doi.org/10.1029/97JD03582>, 1998.
- 645 Iversen, T. and Joranger, E.: Arctic air pollution and large scale atmospheric flows, *Atmospheric Environment* (1967),
646 19, 2099–2108, [https://doi.org/10.1016/0004-6981\(85\)90117-9](https://doi.org/10.1016/0004-6981(85)90117-9), 1985.
- 647 Jacob, D. J., Crawford, J. H., Maring, H., Clarke, A. D., Dibb, J. E., Emmons, L. K., Ferrare, R. A., Hostetler, C. A.,
648 Russell, P. B., Singh, H. B., Thompson, A. M., Shaw, G. E., McCauley, E., Pederson, J. R., and Fisher, J. A.: The
649 Arctic Research of the Composition of the Troposphere from Aircraft and Satellites (ARCTAS) mission: design,
650 execution, and first results, 10, 5191–5212, <https://doi.org/10.5194/acp-10-5191-2010>, 2010.
- 651 Janssens-Maenhout, G., Crippa, M., Guizzardi, D., Dentener, F., Muntean, M., Pouliot, G., Keating, T., Zhang, Q.,
652 Kurokawa, J., Wankmüller, R., Denier van der Gon, H., Kuenen, J. J. P., Klimont, Z., Frost, G., Darras, S., Koffi, B.,
653 and Li, M.: HTAP_v2.2: a mosaic of regional and global emission grid maps for 2008 and 2010 to study hemispheric
654 transport of air pollution, 15, 11411–11432, <https://doi.org/10.5194/acp-15-11411-2015>, 2015.
- 655 Komhyr, W. D., Gammon, R. H., Harris, T. B., Waterman, L. S., Conway, T. J., Taylor, W. R., and Thoning, K. W.:
656 Global atmospheric CO₂ distribution and variations from 1968–1982 NOAA/GMCC CO₂ flask sample data, 90,
657 5567–5596, <https://doi.org/10.1029/JD090iD03p05567>, 1985.
- 658 Kort, E. A., Smith, M. L., Murray, L. T., Gvakharia, A., Brandt, A. R., Peischl, J., Ryerson, T. B., Sweeney, C., and
659 Travis, K.: Fugitive emissions from the Bakken shale illustrate role of shale production in global ethane shift, 43,
660 4617–4623, <https://doi.org/10.1002/2016GL068703>, 2016.
- 661 Kramer, L. J., Helmig, D., Burkhart, J. F., Stohl, A., Oltmans, S., and Honrath, R. E.: Seasonal variability of
662 atmospheric nitrogen oxides and non-methane hydrocarbons at the GEOSummit station, Greenland, 15, 6827–6849,
663 <https://doi.org/10.5194/acp-15-6827-2015>, 2015.
- 664 Lassman, W., Ford, B., Gan, R. W., Pfister, G., Magzamen, S., Fischer, E. V., and Pierce, J. R.: Spatial and temporal
665 estimates of population exposure to wildfire smoke during the Washington state 2012 wildfire season using blended
666 model, satellite, and in situ data, 1, 106–121, <https://doi.org/10.1002/2017GH000049>, 2017.
- 667 Law, K. S., Stohl, A., Quinn, P. K., Brock, C., Burkhart, J., Paris, J.-D., Ancellet, G., Singh, H. B., Roiger, A.,
668 Schlager, H., Dibb, J., Jacob, D. J., Arnold, S. R., Pelon, J., and Thomas, J. L.: Arctic Air Pollution: New Insights
669 from POLARCAT-IPY, <https://doi.org/10.1175/BAMS-D-13-00017.1>, 2014.
- 670 Lelieveld, J., Dentener, F. J., Peters, W., and Krol, M. C.: On the role of hydroxyl radicals in the self-cleansing capacity
671 of the troposphere, 4, 2337–2344, <https://doi.org/10.5194/acp-4-2337-2004>, 2004.
- 672 Levy, H.: Normal Atmosphere: Large Radical and Formaldehyde Concentrations Predicted, 173, 141–143,
673 <https://doi.org/10.1126/science.173.3992.141>, 1971.
- 674 Logan, J. A., Prather, M. J., Wofsy, S. C., and McElroy, M. B.: Tropospheric chemistry: A global perspective, 86,
675 7210–7254, <https://doi.org/10.1029/JC086iC08p07210>, 1981.
- 676 Masarie, K. A. and Tans, P. P.: Extension and integration of atmospheric carbon dioxide data into a globally consistent
677 measurement record, 100, 11593–11610, <https://doi.org/10.1029/95JD00859>, 1995.
- 678 Miller, B. R., Weiss, R. F., Salameh, P. K., Tanhua, T., Grealley, B. R., Mühle, J., and Simmonds, P. G.: Medusa: A
679 Sample Preconcentration and GC/MS Detector System for in Situ Measurements of Atmospheric Trace Halocarbons,
680 Hydrocarbons, and Sulfur Compounds, *Anal. Chem.*, 80, 1536–1545, <https://doi.org/10.1021/ac702084k>, 2008.
- 681 Miller, J. B., Mack, K. A., Dissly, R., White, J. W. C., Dlugokencky, E. J., and Tans, P. P.: Development of analytical
682 methods and measurements of ¹³C/¹²C in atmospheric CH₄ from the NOAA Climate Monitoring and Diagnostics
683 Laboratory Global Air Sampling Network, 107, ACH 11-1-ACH 11-15, <https://doi.org/10.1029/2001JD000630>, 2002.



- 684 Montzka, S. A., Dutton, G. S., Yu, P., Ray, E., Portmann, R. W., Daniel, J. S., Kuijpers, L., Hall, B. D., Mondeel, D.,
685 Siso, C., Nance, J. D., Rigby, M., Manning, A. J., Hu, L., Moore, F., Miller, B. R., and Elkins, J. W.: An unexpected
686 and persistent increase in global emissions of ozone-depleting CFC-11, 557, 413–417, [https://doi.org/10.1038/s41586-](https://doi.org/10.1038/s41586-018-0106-2)
687 018-0106-2, 2018.
- 688 Naik, V., Voulgarakis, A., Fiore, A. M., Horowitz, L. W., Lamarque, J.-F., Lin, M., Prather, M. J., Young, P. J.,
689 Bergmann, D., Cameron-Smith, P. J., Cionni, I., Collins, W. J., Dalsøren, S. B., Doherty, R., Eyring, V., Faluvegi, G.,
690 Folberth, G. A., Josse, B., Lee, Y. H., MacKenzie, I. A., Nagashima, T., van Noije, T. P. C., Plummer, D. A., Righi,
691 M., Rumbold, S. T., Skeie, R., Shindell, D. T., Stevenson, D. S., Strode, S., Sudo, K., Szopa, S., and Zeng, G.:
692 Preindustrial to present-day changes in tropospheric hydroxyl radical and methane lifetime from the Atmospheric
693 Chemistry and Climate Model Intercomparison Project (ACCMIP), 13, 5277–5298, [https://doi.org/10.5194/acp-13-](https://doi.org/10.5194/acp-13-5277-2013)
694 5277-2013, 2013.
- 695 Naus, S., Montzka, S. A., Patra, P. K., and Krol, M. C.: A 3D-model inversion of methyl chloroform to constrain the
696 atmospheric oxidative capacity, 1–23, <https://doi.org/10.5194/acp-2020-624>, 2020.
- 697 Nisbet, E. G., Dlugokencky, E. J., and Bousquet, P.: Methane on the Rise—Again, 343, 493–495,
698 <https://doi.org/10.1126/science.1247828>, 2014.
- 699 Nisbet, E. G., Manning, M. R., Dlugokencky, E. J., Fisher, R. E., Lowry, D., Michel, S. E., Myhre, C. L., Platt, S. M.,
700 Allen, G., Bousquet, P., Brownlow, R., Cain, M., France, J. L., Hermansen, O., Hossaini, R., Jones, A. E., Levin, I.,
701 Manning, A. C., Myhre, G., Pyle, J. A., Vaughn, B. H., Warwick, N. J., and White, J. W. C.: Very Strong Atmospheric
702 Methane Growth in the 4 Years 2014–2017: Implications for the Paris Agreement, 33, 318–342,
703 <https://doi.org/10.1029/2018GB006009>, 2019.
- 704 Oltmans, S., Cheadle, L. C., Helmig, D., Angot, H., Pétron, G., Montzka, S. A., Dlugokencky, E. J., Miller, B., Kofler,
705 J., Hall, B., Andrews, A., Schnell, R. C., and Tans, P.: Atmospheric oil and natural gas hydrocarbon concentration
706 trends in the Northern Colorado Front Range are notably smaller than inventory emissions reductions, *Elementa:*
707 *Science of the Anthropocene*, in review.
- 708 Pekney, N. J., Davidson, C. I., Zhou, L., and Hopke, P. K.: Application of PSCF and CPF to PMF-Modeled Sources
709 of PM_{2.5} in Pittsburgh, 40, 952–961, <https://doi.org/10.1080/02786820500543324>, 2006.
- 710 Perrone, M. G., Vratolis, S., Georgieva, E., Török, S., Šega, K., Veleva, B., Osán, J., Bešlić, I., Kertész, Z., Pernigotti,
711 D., Eleftheriadis, K., and Belis, C. A.: Sources and geographic origin of particulate matter in urban areas of the Danube
712 macro-region: The cases of Zagreb (Croatia), Budapest (Hungary) and Sofia (Bulgaria), *Sci Total Environ*, 619–620,
713 1515–1529, <https://doi.org/10.1016/j.scitotenv.2017.11.092>, 2018.
- 714 Pétron, G., Frost, G., Miller, B. R., Hirsch, A. I., Montzka, S. A., Karion, A., Trainer, M., Sweeney, C., Andrews, A.
715 E., Miller, L., Kofler, J., Bar-Ilan, A., Dlugokencky, E. J., Patrick, L., Moore, C. T., Ryerson, T. B., Siso, C., Kolodzey,
716 W., Lang, P. M., Conway, T., Novelli, P., Masarie, K., Hall, B., Guenther, D., Kitzis, D., Miller, J., Welsh, D., Wolfe,
717 D., Neff, W., and Tans, P.: Hydrocarbon emissions characterization in the Colorado Front Range: A pilot study, 117,
718 <https://doi.org/10.1029/2011JD016360>, 2012.
- 719 Pétron, G., Karion, A., Sweeney, C., Miller, B. R., Montzka, S. A., Frost, G. J., Trainer, M., Tans, P., Andrews, A.,
720 Kofler, J., Helmig, D., Guenther, D., Dlugokencky, E., Lang, P., Newberger, T., Wolter, S., Hall, B., Novelli, P.,
721 Brewer, A., Conley, S., Hardesty, M., Banta, R., White, A., Noone, D., Wolfe, D., and Schnell, R.: A new look at
722 methane and nonmethane hydrocarbon emissions from oil and natural gas operations in the Colorado Denver-
723 Julesburg Basin, 119, 6836–6852, <https://doi.org/10.1002/2013JD021272>, 2014.
- 724 G2401 Gas Concentration Analyzer | Picarro: https://www.picarro.com/products/g2401_gas_concentration_analyzer,
725 last access: 31 March 2020.
- 726 Pollmann, J., Helmig, D., Hueber, J., Plass-Dülmer, C., and Tans, P.: Sampling, storage, and analysis of C₂–C₇ non-
727 methane hydrocarbons from the US National Oceanic and Atmospheric Administration Cooperative Air Sampling



- 728 Network glass flasks, *Journal of Chromatography A*, 1188, 75–87, <https://doi.org/10.1016/j.chroma.2008.02.059>,
729 2008.
- 730 Arctic Oil & Gas Development: The Case of Greenland: [https://arcticyearbook.com/arctic-yearbook/2018/2018-](https://arcticyearbook.com/arctic-yearbook/2018/2018-scholarly-papers/285-arctic-oil-gas-development-the-case-of-greenland)
731 [scholarly-papers/285-arctic-oil-gas-development-the-case-of-greenland](https://arcticyearbook.com/arctic-yearbook/2018/2018-scholarly-papers/285-arctic-oil-gas-development-the-case-of-greenland), last access: 25 November 2020.
- 732 Pozzer, A., Pollmann, J., Taraborrelli, D., Jöckel, P., Helmig, D., Tans, P., Hueber, J., and Lelieveld, J.: Observed and
733 simulated global distribution and budget of atmospheric C₂-C₅ alkanes, 10, 4403–4422, [https://doi.org/10.5194/acp-](https://doi.org/10.5194/acp-10-4403-2010)
734 [10-4403-2010](https://doi.org/10.5194/acp-10-4403-2010), 2010.
- 735 Rex, D. F.: Blocking Action in the Middle Troposphere and its Effect upon Regional Climate, 2, 275–301,
736 <https://doi.org/10.1111/j.2153-3490.1950.tb00339.x>, 1950.
- 737 Greenland Opens Offshore Areas for Drilling:
738 https://www.rigzone.com/news/greenland_opens_offshore_areas_for_drilling-05-nov-2020-163772-article/, last
739 access: 25 November 2020.
- 740 Rudolph, J.: The tropospheric distribution and budget of ethane, 100, 11369–11381,
741 <https://doi.org/10.1029/95JD00693>, 1995.
- 742 Scanlon, J. T. and Willis, D. E.: Calculation of Flame Ionization Detector Relative Response Factors Using the
743 Effective Carbon Number Concept, *J Chromatogr Sci*, 23, 333–340, <https://doi.org/10.1093/chromsci/23.8.333>, 1985.
- 744 von Schneidmesser, E., Monks, P. S., and Plass-Duelmer, C.: Global comparison of VOC and CO observations in
745 urban areas, *Atmospheric Environment*, 44, 5053–5064, <https://doi.org/10.1016/j.atmosenv.2010.09.010>, 2010.
- 746 Schultz, M. G., Akimoto, H., Bottenheim, J., Buchmann, B., Galbally, I. E., Gilge, S., Helmig, D., Koide, H., Lewis,
747 A. C., Novelli, P. C., Dülmer, C. P., Ryerson, T. B., Steinbacher, M., Steinbrecher, R., Tarasova, O., Tørseth, K.,
748 Thouret, V., and Zellweger, C.: The Global Atmosphere Watch reactive gases measurement network, 3, 000067,
749 <https://doi.org/10.12952/journal.elementa.000067>, 2015.
- 750 Sicotte, D. M.: From cheap ethane to a plastic planet: Regulating an industrial global production network, *Energy*
751 *Research & Social Science*, 66, 101479, <https://doi.org/10.1016/j.erss.2020.101479>, 2020.
- 752 Simpson, I. J., Andersen, M. P. S., Meinardi, S., Bruhwiler, L., Blake, N. J., Helmig, D., Rowland, F. S., and Blake,
753 D. R.: Long-term decline of global atmospheric ethane concentrations and implications for methane, *Nature*, 488,
754 490–494, <https://doi.org/10.1038/nature11342>, 2012.
- 755 Spivakovsky, C. M., Logan, J. A., Montzka, S. A., Balkanski, Y. J., Foreman-Fowler, M., Jones, D. B. A., Horowitz,
756 L. W., Fusco, A. C., Brenninkmeijer, C. a. M., Prather, M. J., Wofsy, S. C., and McElroy, M. B.: Three-dimensional
757 climatological distribution of tropospheric OH: Update and evaluation, 105, 8931–8980,
758 <https://doi.org/10.1029/1999JD901006>, 2000.
- 759 Steele, L. P.: Atmospheric Methane Concentrations, the NOAA/CMDL Global Cooperative Flask Sampling Network,
760 1983-1988, Oak Ridge National Laboratory, 324 pp., 1991.
- 761 Steele, L. P., Fraser, P. J., Rasmussen, R. A., Khalil, M. A. K., Conway, T. J., Crawford, A. J., Gammon, R. H.,
762 Masarie, K. A., and Thoning, K. W.: The global distribution of methane in the troposphere, *J Atmos Chem*, 5, 125–
763 171, <https://doi.org/10.1007/BF00048857>, 1987.
- 764 Tanner, D., Helmig, D., Hueber, J., and Goldan, P.: Gas chromatography system for the automated, unattended, and
765 cryogen-free monitoring of C₂ to C₆ non-methane hydrocarbons in the remote troposphere, *Journal of*
766 *Chromatography A*, 1111, 76–88, <https://doi.org/10.1016/j.chroma.2006.01.100>, 2006.



- 767 Thompson, A. M.: The Oxidizing Capacity of the Earth's Atmosphere: Probable Past and Future Changes, 256, 1157–
768 1165, <https://doi.org/10.1126/science.256.5060.1157>, 1992.
- 769 Thoning, K. W., Tans, P. P., and Komhyr, W. D.: Atmospheric carbon dioxide at Mauna Loa Observatory: 2. Analysis
770 of the NOAA GMCC data, 1974–1985, 94, 8549–8565, <https://doi.org/10.1029/JD094iD06p08549>, 1989.
- 771 Trolier, M., White, J. W. C., Tans, P. P., Masarie, K. A., and Gemery, P. A.: Monitoring the isotopic composition of
772 atmospheric CO₂: Measurements from the NOAA Global Air Sampling Network, 101, 25897–25916,
773 <https://doi.org/10.1029/96JD02363>, 1996.
- 774 Tzompa-Sosa, Z. A., Mahieu, E., Franco, B., Keller, C. A., Turner, A. J., Helmig, D., Fried, A., Richter, D., Weibring,
775 P., Walega, J., Yacovitch, T. I., Herndon, S. C., Blake, D. R., Hase, F., Hannigan, J. W., Conway, S., Strong, K.,
776 Schneider, M., and Fischer, E. V.: Revisiting global fossil fuel and biofuel emissions of ethane, 122, 2493–2512,
777 <https://doi.org/10.1002/2016JD025767>, 2017.
- 778 Tzompa-Sosa, Z. A., Henderson, B. H., Keller, C. A., Travis, K., Mahieu, E., Franco, B., Estes, M., Helmig, D., Fried,
779 A., Richter, D., Weibring, P., Walega, J., Blake, D. R., Hannigan, J. W., Ortega, I., Conway, S., Strong, K., and
780 Fischer, E. V.: Atmospheric Implications of Large C₂-C₅ Alkane Emissions From the U.S. Oil and Gas Industry, 124,
781 1148–1169, <https://doi.org/10.1029/2018JD028955>, 2019.
- 782 U.S. Field Production of Natural Gas Liquids:
783 https://www.eia.gov/dnav/pet/hist/LeafHandler.ashx?n=PET&s=M_EPL2_FPF_NUS_MBBL&f=A, last access: 8
784 March 2021.
- 785 U.S. Field Production of Propane:
786 https://www.eia.gov/dnav/pet/hist/LeafHandler.ashx?n=PET&s=M_EPLLPA_FPF_NUS_MBBL&f=M, last access:
787 8 March 2021.
- 788 Val Martin, M., Heald, C. L., Ford, B., Prenni, A. J., and Wiedinmyer, C.: A decadal satellite analysis of the origins
789 and impacts of smoke in Colorado, 2013.
- 790 Warneke, C., Gouw, J. A. de, Holloway, J. S., Peischl, J., Ryerson, T. B., Atlas, E., Blake, D., Trainer, M., and Parrish,
791 D. D.: Multiyear trends in volatile organic compounds in Los Angeles, California: Five decades of decreasing
792 emissions, 117, <https://doi.org/10.1029/2012JD017899>, 2012.
- 793 Warner, M. S. C.: Introduction to PySPLIT: A Python Toolkit for NOAA ARL's HYSPLIT Model, 20, 47–62,
794 <https://doi.org/10.1109/MCSE.2017.3301549>, 2018.
- 795 Wiedinmyer, C., Akagi, S. K., Yokelson, R. J., Emmons, L. K., Al-Saadi, J. A., Orlando, J. J., and Soja, A. J.: The
796 Fire INventory from NCAR (FINN): a high resolution global model to estimate the emissions from open burning, 4,
797 625–641, <https://doi.org/10.5194/gmd-4-625-2011>, 2011.
- 798 Wiedinmyer, C., Kumra, Y., McDonald-Buller, E. C., Seto, K., Emmons, L. K., Buccholz, R., Tang, W., Joseph, M.,
799 Barsanti, K., Carlton, A. M., and Yokelson, R. J.: The Fire Inventory from NCAR version 2: an updated global fire
800 emissions model for climate and chemistry applications., *Journal of Advances in Modeling Earth Systems*, in prep.
- 801 WMO: GAW Report, 171. A WMO/GAW Expert Workshop on Global Long-term Measurements of Volatile Organic
802 Compounds, WMO, Geneva, 36 p. pp., 2007.
- 803 Wofsy, S. C., Afshar, S., Allen, H. M., Apel, E. C., Asher, E. C., Barletta, B., Bent, J., Bian, H., Biggs, B. C., Blake,
804 D. R., Blake, N., Bourgeois, I., Brock, C. A., Brune, W. H., Budney, J. W., Bui, T. P., Butler, A., Campuzano-Jost,
805 P., Chang, C. S., Chin, M., Commane, R., Correa, G., Crounse, J. D., Cullis, P. D., Daube, B. C., Day, D. A., Dean-
806 Day, J. M., Dibb, J. E., Digangi, J. P., Diskin, G. S., Dollner, M., Elkins, J. W., Erdesz, F., Fiore, A. M., Flynn, C. M.,
807 Froyd, K. D., Gesler, D. W., Hall, S. R., Hanisco, T. F., Hannun, R. A., Hills, A. J., Hints, E. J., Hoffman, A.,
808 Hornbrook, R. S., Huey, L. G., Hughes, S., Jimenez, J. L., Johnson, B. J., Katich, J. M., Keeling, R. F., Kim, M. J.,



- 809 Kupc, A., Lait, L. R., Lamarque, J.-F., Liu, J., Mckain, K., Mclaughlin, R. J., Meinardi, S., Miller, D. O., Montzka, S.
810 A., Moore, F. L., Morgan, E. J., Murphy, D. M., Murray, L. T., Nault, B. A., Neuman, J. A., Newman, P. A., Nicely,
811 J. M., Pan, X., Paplawsky, W., Peischl, J., Prather, M. J., Price, D. J., Ray, E. A., Reeves, J. M., Richardson, M.,
812 Rollins, A. W., Rosenlof, K. H., Ryerson, T. B., Scheuer, E., Schill, G. P., Schroder, J. C., Schwarz, J. P., St. Clair, J.
813 M., Steenrod, S. D., Stephens, B. B., Strode, S. A., Sweeney, C., Tanner, D., Teng, A. P., Thames, A. B., Thompson,
814 C. R., Ullmann, K., Veres, P. R., Vizenor, N., Wagner, N. L., Watt, A., Weber, R., Weinzierl, B., et al.: ATom: Merged
815 Atmospheric Chemistry, Trace Gases, and Aerosols, <https://doi.org/10.3334/ORNLDAAC/1581>, 2018.
- 816 Worton, D. R., Sturges, W. T., Reeves, C. E., Newland, M. J., Penkett, S. A., Atlas, E., Stroud, V., Johnson, K.,
817 Schmidbauer, N., Solberg, S., Schwander, J., and Barnola, J.-M.: Evidence from firm air for recent decreases in non-
818 methane hydrocarbons and a 20th century increase in nitrogen oxides in the northern hemisphere, *Atmospheric*
819 *Environment*, 54, 592–602, <https://doi.org/10.1016/j.atmosenv.2012.02.084>, 2012.
- 820 Xiao, Y., Logan, J. A., Jacob, D. J., Hudman, R. C., Yantosca, R., and Blake, D. R.: Global budget of ethane and
821 regional constraints on U.S. sources, 113, <https://doi.org/10.1029/2007JD009415>, 2008.
- 822 Yu, Y., Hung, H., Alexandrou, N., Roach, P., and Nordin, K.: Multiyear Measurements of Flame Retardants and
823 Organochlorine Pesticides in Air in Canada's Western Sub-Arctic, *Environ. Sci. Technol.*, 49, 8623–8630,
824 <https://doi.org/10.1021/acs.est.5b01996>, 2015.
- 825 Zhou, H., Hopke, P. K., Zhou, C., and Holsen, T. M.: Ambient mercury source identifications at a New York State
826 urban site: Rochester, NY, *Science of The Total Environment*, <https://doi.org/10.1016/j.scitotenv.2018.09.040>, 2018.
- 827 Zong, Z., Wang, X., Tian, C., Chen, Y., Fu, S., Qu, L., Ji, L., Li, J., and Zhang, G.: PMF and PSCF based source
828 apportionment of PM_{2.5} at a regional background site in North China, *Atmospheric Research*, 203, 207–215,
829 <https://doi.org/10.1016/j.atmosres.2017.12.013>, 2018.
- 830



Table 1: Rates of change and 95 % confidence interval (in brackets) inferred from discrete sampling (in ppt per year). ALT, BRW, MHD, LEF, and KUM refer to Alert, Utqiagvik/Barrow, Mace Head, Park Falls, and Cape Kumukahi. The localization of the sites can be found in Figure 1. The symbols shown next to each rate of change relate to how statistically significant the estimate is: $p < 0.001 = ***$, $p < 0.01 = **$, and $p < 0.05 = *$.

Site	2010-2014	2015-2018
Ethane		
ALT	+52.8 [+32.7, +73.0] ***	-56.9 [-79.9, -36.6] ***
BRW	+40.5 [+25.9, +59.1] ***	-50.6 [-69.4, -27.6] ***
KUM	+18.4 [+7.9, +29.5] ***	-43.1 [-62.1, -28.1] ***
LEF	+167.7 [+157.5, +186.0] ***	-247.8 [-312.2, -158.2] ***
MHD	+51.8 [+44.4, +63.2] ***	-18.6 [-102.6, +45.4]
Propane		
ALT	+24.8 [+16.5, +37.7] ***	-55.6 [-65.1, -45.9] ***
BRW	+14.5 [+9.1, +20.2] ***	-35.1 [-45.3, -25.6] ***
KUM	+3.1 [+0.2, +5.9] *	-13.2 [-15.9, -10.7] ***
LEF	+89.8 [+68.5, +123.5] ***	-110.0 [-173.6, -75.6] ***
MHD	+21.3 [+16.9, +27.1] ***	-24.2 [-56.2, -7.2] **



Figure 1: Location of the Greenland Environmental Observatory at Summit station (red dot, SUM) where long-term in-situ monitoring was carried out, and of Alert (ALT), Utqiagvik (formerly known as Barrow (BRW)), Mace Head (MHD), Park Falls (LEF), and Cape Kumukahi (KUM), where discrete samples were collected by both the NOAA/ESRL/GML CCGG and HATS sampling networks. The map is centered over the North Pole.

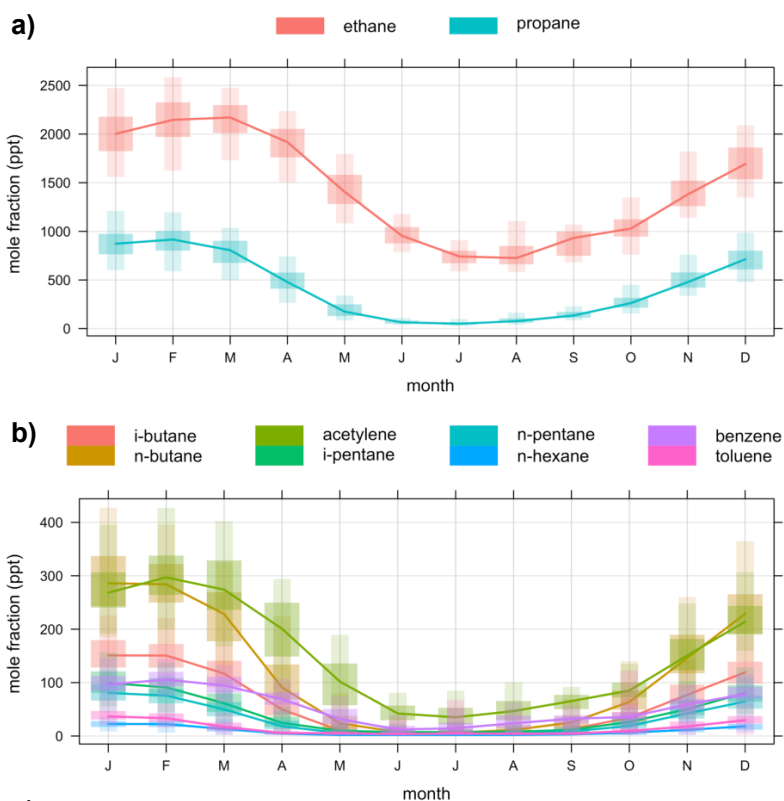


Figure 2: Monthly variation of **a)** ethane and propane, and **b)** C₄-C₇ non-methane hydrocarbons measured in ambient air at GEOSummit as inferred from 2008-2010 and 2012-2020 in-situ measurements. In the monthly boxplots, the lower and upper end of the box correspond to the 25th and 75th percentiles while the whiskers extend from the 5th to the 95th percentiles.

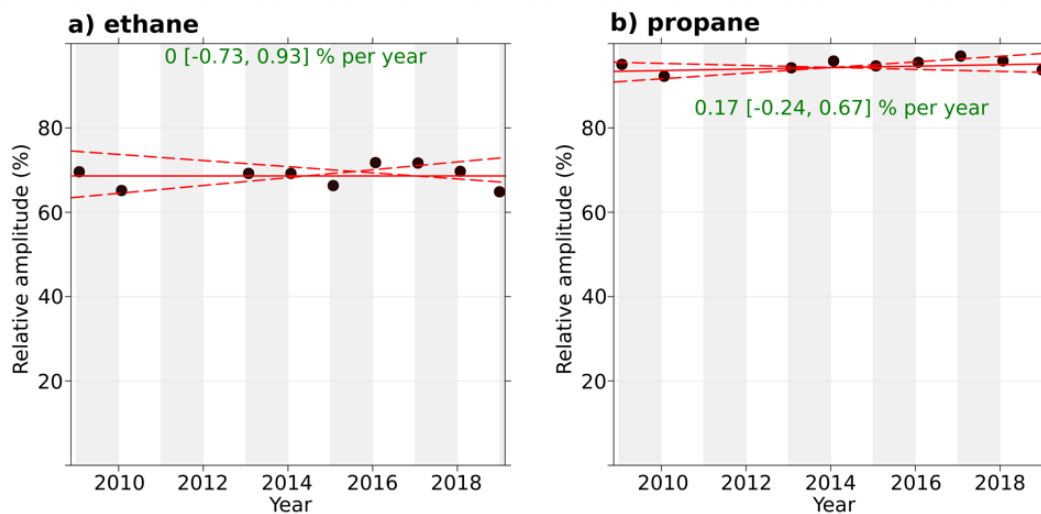


Figure 3: Trend in peak-to-minimum seasonal amplitude of **a)** ethane and **b)** propane at GEOSummit, calculated as the relative difference between the maximum and minimum values from the smooth curve for each annual cycle. The solid red line shows the trend estimate and the dashed red lines show the 95 % confidence interval for the trend based on resampling methods. The overall trend is shown at the top along with the 95 % confidence interval in the slope.

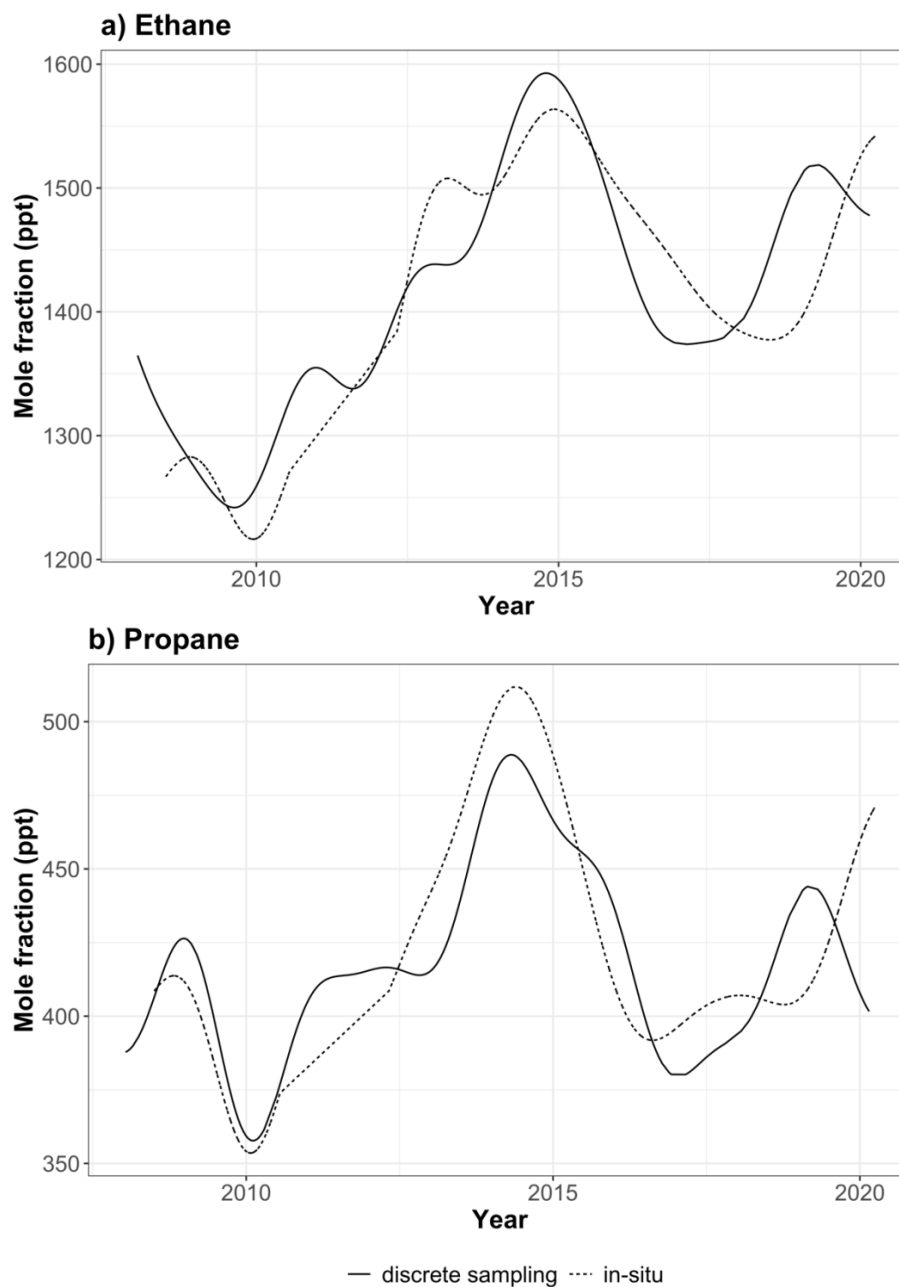


Figure 4: a) Ethane, and b) propane trends at GEOSummit from July 2008 to March 2020. Trends inferred from in-situ and discrete sampling are shown by the dotted and solid lines, respectively.

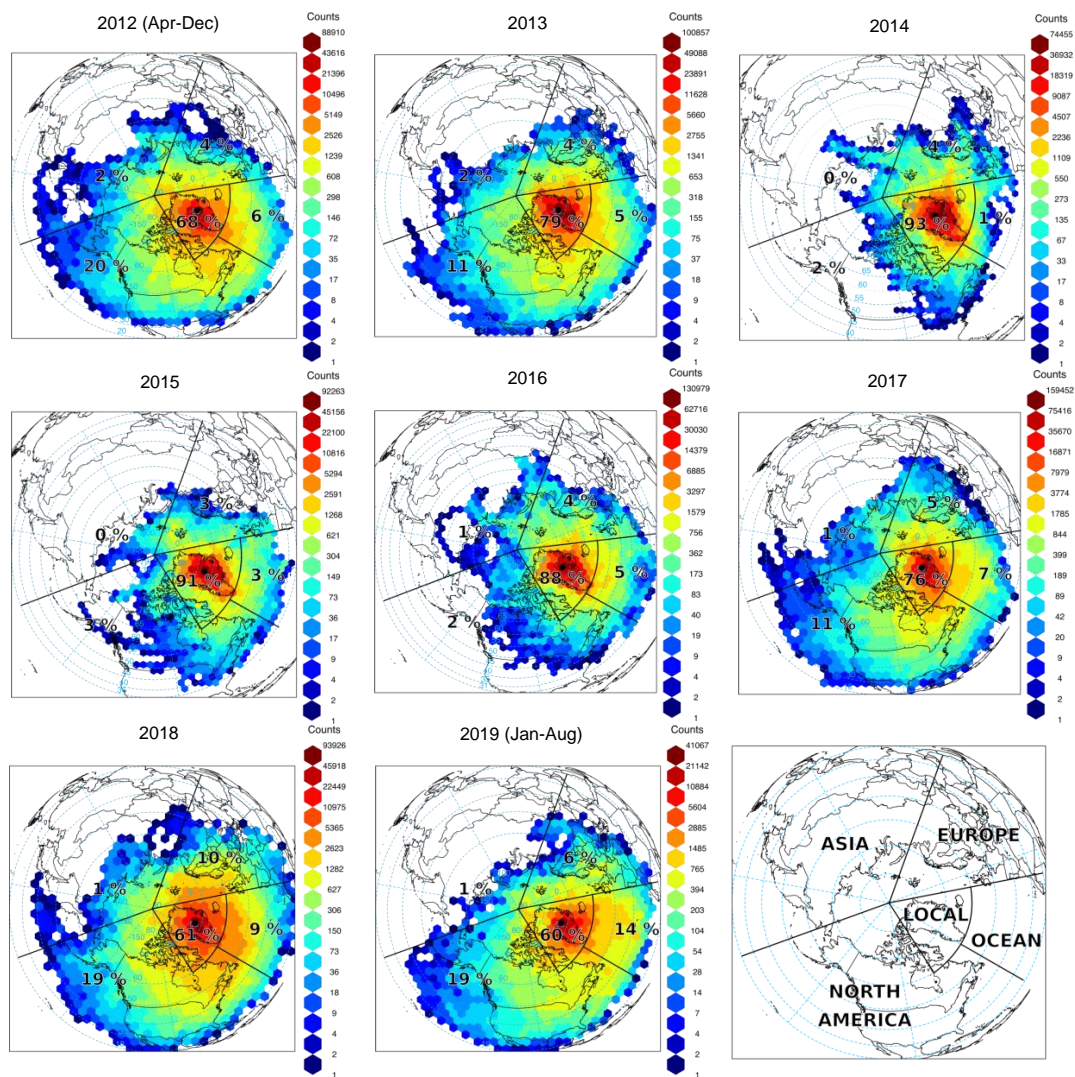


Figure 5: Origin air masses influencing GEOSummit (black dot). Gridded back trajectory frequencies using an orthogonal map projection (centered over the North Pole) with hexagonal binning. The tiles represent the number of incidences and the numbers the relative influence of the various sectors.



Figure 6: a) Annual relative contribution of different geographical sectors to air masses influencing GEOSummit according to the HYSPLIT back-trajectories analysis. b) Annual biomass burning emissions (in mole/year) from all open burning north of 45°N according to the Fire INventory from NCAR (FINNv2.2) emission estimates (MODIS only).

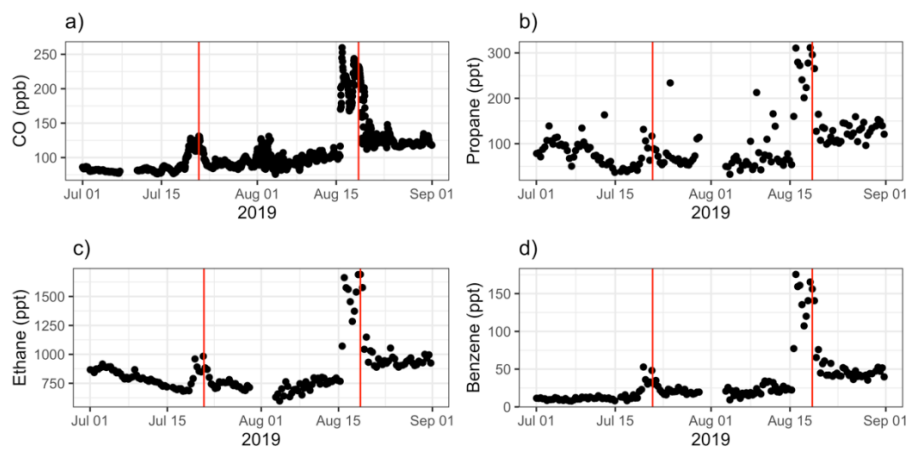


Figure 7: Time-series of **a)** carbon monoxide (CO), **b)** propane, **c)** ethane, and **d)** benzene mixing ratios in ambient air at GEOSummit in July-August 2019. The two vertical red lines show the simultaneous enhancement of mixing ratios in two biomass burning plumes.

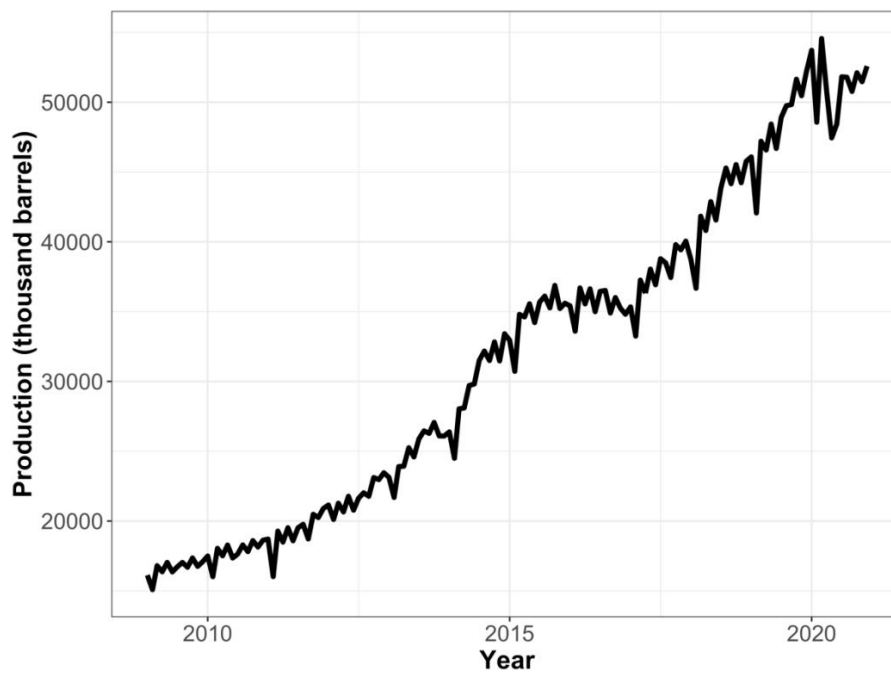


Figure 8: U.S. field production of propane in thousand barrels per month. Data courtesy of the U.S. Energy Information Administration. The production temporarily plateaued from June 2014 to December 2016.